Dynamic characteristics analysis of locomotive traction gear pair system under internal and external excitations

Yan Xia, Yi Wan, Hongwei Wang and Zhanqiang Liu
Key Laboratory of High Efficiency and Clean Manufacturing, Ministry of Education, School of Mechanical Engineering, Shandong University, Jinan, China and National Demonstration Center for Experimental Mechanical Engineering Education, Shandong University, Jinan, China

Received 3 March 2019
Revised 4 August 2019
9 February 2020
Accepted 11 February 2020

Abstract

Purpose – As the transmission component of a locomotive, the traction gear pair system has a direct effect on the stability and reliability of the whole machine. This paper aims to provide a detailed dynamic analysis for the traction system under internal and external excitations by numerical simulation.

Design/methodology/approach – A non-linear dynamic model of locomotive traction gear pair system is proposed, where the comprehensive time-varying meshing stiffness is obtained through the Ishikawa formula method and verified by the energy method, and then the sliding friction excitation is analyzed based on the location of the contact line. Meantime, the adhesion torque is constructed as a function of the adhesion-slip feature between wheelset and rail. Through Runge–Kutta numerical method, the system responses are studied with varying bifurcation parameters consisting of exciting frequency, load fluctuation, gear backlash, error fluctuation and friction coefficient. The dynamic behaviors of the system are analyzed and discussed from bifurcation diagram, time history, spectrum plot, phase portrait, Poincaré map and three-dimensional frequency spectrum.

Findings – The analysis results reveal that as control parameters vary the system experiences complex transition among a diverse range of motion states such as one-periodic, multi-periodic and chaotic motions. Specifically, the significant difference in system bifurcation characteristics can be observed under different adhesion conditions. The suitable gear backlash and error fluctuation can avoid the chaotic motion, and thus, reduce the vibration amplitude of the system. Similarly, the increasing friction coefficient can also suppress the unstable state and improve the stability of the system.

Originality/value – The numerical results may provide a systemic understanding of dynamic characteristics and present some available information to design and optimize the transmission performance of the locomotive traction system.

Keywords Sliding friction, Bifurcation, Nonlinear dynamics, Adhesion torque, Locomotive, Traction gear pair system

Paper type Research paper

This study was funded by a major project of scientific and technological innovation in Shandong Province (2017CXGC0917) and The Fundamental Research Funds of Shandong University (2017JC041). Meantime, the first author is also grateful to the support from China Association for Science and Technology and China Scholarship Council.

Declaration of interest: there is no potential conflict of interest concerning the paper the authors report.

Engineering Computations
Vol. 37 No. 8, 2020
pp. 2587-2617

0264-4401
DOI 10.1108/EC-03-2019-0083

Nomenclature

$\theta i, Ii$	= angular displacement and moment of inertia of two gears;
r_{bi}, r_{ai}, r_i	= radius of base, addendum and pitch circles of two gears;
$c_m, k(t), F_j$	= meshing damping, time-varying meshing stiffness and meshing force of gear pair;
F_f, F_w	= sliding friction force and adhesion force;
T_1, T_2	= driving torque and adhesion torque;
$\delta_{Br}, \delta_{Bt}, \delta_S, \delta_G, \delta_p$	= bending deformation of rectangular portion, bending deformation of trapezoidal part, shear deformation, sloping deformation and contact deformation;
E, B,v	= Young's modulus, face width and Poisson's ratio;
F_n	= load in normal plane;
$k_1(t), k_1(\tau), k_2(t), k_2(\tau)$	= meshing stiffness and the corresponding dimensionless stiffness in single or double teeth meshing area;
$k_{2m}, k_{1m}, a_{2(1)}, b_{2(1)}$	= Fourier series coefficient of dimensionless meshing stiffness;
t_m, t_d, t_s	= meshing period, double-tooth meshing period and single-tooth meshing period;
ζ, ε	= proportionality coefficient and contact ratio;
$U, U_h, U_b, U_a, U_s, U_f$	= total potential energy, Hertzian energy, bending energy, shear energy energy, axial compressive energy and gear fillet-foundation energy;
k_h, k_b, k_s, k_a, k_f	= Hertzian stiffness, bending stiffness, shear stiffness, axial compressive stiffness and gear fillet-foundation stiffness;
$e(t), e_m, e_a$	= meshing transmission error, mean value and fluctuation value;
$b, f(x)$	= half of backlash, non-linear displacement function;
l_{j1}, l_{j2}	= frictional force arms of two gears;
S_j	= moved distance of the j-th pair of teeth;
N	= maximum value of meshing teeth at the same time;
$\lambda_j, \mu_B,$	= direction coefficient of friction force and coefficient of sliding friction;
T_{f1}, T_{f2}	= friction moments of two gears;
R, Q, ω, v_L	= radius, mass and instantaneous, angular velocity of wheel and driving speed of locomotive;
$s, s_m, \mu, \mu_m, k_\mu$	= creep ratio and critical creep rate, adhesion coefficient and its maximum value and the negative slope of adhesion curve;
m_{e1}, m_{e2}	= equivalent mass of two gears; and
ω_n, τ	= natural frequency and dimensionless time.

1. Introduction

With the accelerating demands of high speed, heavy load and low vibration in railway transportation, the safe operation of the locomotive is facing serious challenges. Traction gear pair system as the key component of locomotive directly influences the dynamic performance and stability of the entire train (Zhang *et al.*, 2019a, 2019b). Because of the internal and external excitations, the traction device is a complex system with strong non-linearity, which may become unpredictable and uncontrollable excited by vibration response. Based on these traits, there is a demand to gain a thorough understanding of the dynamic behaviors of the traction gear pair system in the locomotive. In this study, we focus on the comprehensive analysis of a typical traction gear pair system under internal and external excitations, to provide some guidance for the design and control of the locomotive traction system.

The dynamics of the gear pair system have been carried out extensively. A torsional model of gear pair system was built by Kahraman and Singh (1990), where the meshing

stiffness was time-invariant in the model. Similarly, Shen *et al.* (2006) built a torsional mathematical model for a spur of gear pair with the consideration of transmission error, meshing stiffness and gear backlash, and then the effects of damping and excitation amplitude on the dynamic behaviors were researched. Based on a purely torsional gear system, Walha *et al.* (2006) analyzed the influence of gear backlash on the dynamic behavior and observed the amplitude jumps phenomenon. Then, Wang *et al.* (2007) performed systematically analysis of the non-linear dynamic characteristics of a hypoid gear pair with non-linearity of backlash and time-invariance. Moradi and Salarieh (2012) investigated the non-linear oscillations of gear pairs with gear backlash. Meantime, the influences of system parameters on the dynamic transmission error amplitude were obtained. Chang-Jian (2013) reported the gear system responses under the non-linear conditions, and the results indicated that the system experienced rich motion states such as periodic, sub-harmonic, quasi-periodic and chaotic responses. Farshidianfar and Saghafi (2014a, 2014b, 2014c) used a torsional dynamics model of a spur gear pair to study first the bifurcation and chaos characteristic and then suppress the chaotic response of gear system by non-feedback control method. The comprehensive analysis of gear system motion states was performed by Li *et al.* (2014) considering time-varying stiffness, backlash, transmission error and external excitation and the effects of control parameters above on system responses were discussed. Accordingly, the previously published papers above focus on the study of dynamics of gear pair with meshing stiffness, transmission error and backlash, where the meshing stiffness is time-invariant sometimes. Furthermore, it is always ignored the effect of tooth surface friction or the coupled interaction between friction and meshing stiffness on the dynamics of the gear system. Vaishya and Singh (2001a, 2001b) established early a single degree-of-freedom dynamic model of gear pair considering friction, while the meshing stiffness was simplified to be a square wave. He *et al.* (2007, 2008) analyzed the influences of friction and meshing stiffness on the transmission error and provided an empirical formula for calculation of friction force. Based on a dynamic model for the gear system with sliding friction, Wang *et al.* (2012) investigated the dynamic behavior with friction and non-friction. However, the friction force in signal and double teeth meshing area could not be considered comprehensively. Wang *et al.* (2017) presented that the friction force was expressed as the product of friction coefficient and meshing force, while the directional coefficient was ignored. According to the above discussions, even though there exists an analysis of the dynamics of the gear system considering meshing stiffness and friction condition in many studies, the meshing stiffness is often simplified and the friction model could not reflect factually the dynamic change of friction force.

Quite a few studies on the dynamics of the locomotive with and without gear transmission system have been investigated in the past few decades. Zhai *et al.* (2013) modeled a fundamental model for dynamics analysis of the train–track–bridge coupled system to predict the dynamic behaviors of the coupled system by computer simulation. Wang *et al.* (2016) proposed an excitation model of rail spalling failure to analyze the characteristics of wheel-rail dynamic vibration according to the theory of vehicle-rail coupled dynamics. In the two papers above, they are concentrated on the analysis of dynamic responses of the vehicle with the effect of external excitations. Apparently, many efforts have been performed in dynamic analysis of locomotive or train considering the effect of the traction gear system. For the purpose of describing the dynamic behaviors for a locomotive with saturated adhesion, Yao *et al.* (2011) used the notions of mean and dynamic slip rate to analyze the stability and characteristics of stick-slip vibration. Subsequently, Yao *et al.* (2015) analyzed the relationship between vibration amplitude and stability of stick-slip vibration, which studied the influences of traction system suspension parameters

on the re-adhesion performance of locomotive. Huang *et al.* (2015) established a dynamic model of motor cars including a traction system to research the influence of the internal excitation of traction system on the dynamic performance of the train, where the meshing stiffness and gear transmission error were taken into account in the model. Considering gear transmissions, Chen *et al.* (2017a) developed a locomotive–rail vertical model, and the dynamic feature of the whole system with the excitations from the wheel–rail and/or the gear mesh interface was carried out by numerical simulations. To research further, the coupling interactions between the gear transmission motion and wheelset, Chen *et al.* (2017b) proposed a locomotive-track vertical-longitudinal coupled dynamic model. Then, the dynamic responses of the locomotive under the tractive conditions were performed by numerical simulation and experimental tests. Recently, with consideration of the dynamic effects of the gear system, Zhang *et al.* (2019a, 2019b) proposed a locomotive-rail coupled spatial dynamic model, in which the dynamic interactions of motions from the power transmission system and locomotive components are comprehensively included. Likewise, there exist some works in terms of dynamics of the traction gear system in railway locomotive. Zhao *et al.* (2009) presented the dynamic models for the locomotive driving system. The self-excited torsional vibration for the traction system was investigated by using MATLAB/SIMULINK. To avoid severe vibration leading to shaft damage, Cao *et al.* (2016) provided a two-mass model of the drive system and researched the influence parameters of vibration frequency and amplitude by simulation. However, the two dynamic models above are unduly simplified into two lumped mass. Wang *et al.* (2017) analyzed the effects of the rotational speed of driving pinion and support stiffness on the dynamic response of the locomotive driving system based on the proposed system model, while the friction force is neglected. In addition, to describe system behaviors, Wang *et al.* (2017) built a simulation model for locomotive traction system with sliding friction and carried out the analysis about the effect of tooth surface friction on system stability. However, the friction excitation is only expressed as the proportional function of the meshing force without consideration direction coefficient.

As mentioned above, it is still necessary to investigate the non-linear dynamics of locomotive traction system considering the effect of excitations including time-varying meshing stiffness, sliding friction and adhesion torque comprehensively though the dynamics of gear pair system or locomotive have studied previously. Thus, the purpose of this study is to propose a dynamic model for locomotive traction gear pair system under internal and external excitations aroused by backlash, transmission error, time-varying meshing stiffness, friction force and adhesion torque, and then use it to analyze the system responses. The differential equation for the traction system is calculated using the Runge–Kutta method. Meantime, the dynamic responses of the system are determined from the bifurcation diagram, time history, spectrum plot, phase portrait, three-dimensional frequency spectrum and Poincaré map. The following structure of this paper is listed: in Section 2, the locomotive traction gear system is described to exhibit its structure type and operating principle. Then, the internal and external excitations are investigated in Section 3 and Section 4, respectively. Subsequently, the dynamic equations of the locomotive traction gear system are derived by Newton's laws of motion in Section 5. Section 6 discusses the non-linear dynamic responses for the traction system of the locomotive with the influences of control parameters. Finally, some brief conclusions are presented in Section 7.

2. Description of locomotive traction gear pair system

The traction gear system of a representative locomotive mostly consists of traction motor, coupling, driving gear, driven gear, wheelset and so forth, which can be seen in Figure 1(a).

As the power part of locomotive, the traction system is used to transmit the driving torque generated by traction motor to wheelset via gear-pair, which makes the locomotive running or braking.

To research the dynamic behavior of the traction gear system conveniently, some assumptions are provided as follows:

- The meshing gears are involute spur gears, in which meshing force is simplified as the spring-damping force and is always in the meshing plane;
- The transmission shafts and bearings that support gears are inflexible; and
- The gears are assumed to be rigid, where only the torsional displacement of gear system is considered.

Then, the simplified traction system model is illustrated in Figure 1(b). In the dynamic model, θ_i, I_i and r_{bi} ($i = 1, 2$) are the angular displacements, the moment of inertia and radius of base circles of the driving and driven gears. c_m and k(t) are the meshing damping and stiffness of gear-pair, respectively. F_f stands for the sliding friction force between the two gears. In addition, T_1 is the driving torque of the gear system, which is considered to keep constant. T_2 represents the load torque, namely, adhesion torque caused by adhesion characteristics between wheelset and rail.

3. Internal excitations

3.1 Time-varying meshing stiffness

During the gear meshing process, the number of meshing tooth varies, leading to the time-varying characteristic of meshing stiffness, which has an important effect on the dynamic response of the gear system. It is the pre-condition of dynamics analysis for gear systems to calculate the time-varying meshing stiffness accurately. At present, there appear several calculation methods of meshing stiffness mainly consisting of Ishikawa method (Shi *et al.*, 2013), finite element method (Tamminana and Kahraman, 2006), energy method (Tian, 2004; Chen and Shao, 2011; Wan *et al.*, 2014) and so forth, which have different characters. The energy method is widely used to obtain the mesh stiffness of the cracked gear system. The finite element method can simulate the meshing process factually, while it will take too much time. In this study, the meshing stiffness of the healthy gear pair is analyzed through the Ishikawa method, which is verified with the energy method.

3.1.1 Calculation meshing stiffness with Ishikawa method. According to Ishikawa method, gear tooth is usually simplified as a cantilever beam that is combined with a

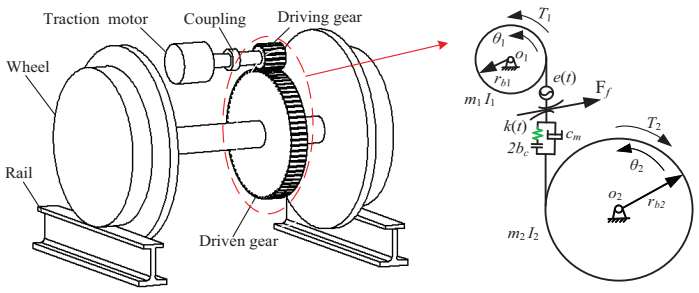

Figure 1.
Structural schematic (a) and the corresponding dynamic model (b) of locomotive traction gear transmission system

trapezoid and a rectangular, in which the length of rectangular is defined as the dangerous section of gear tooth that is calculated by 30-degree tangent method, as shown in Figure 2.

The deformation of the single tooth along the direction of the meshing line can be expressed as:

$$\delta = \delta_{Br} + \delta_{Bt} + \delta_S + \delta_G \tag{1}$$

where δ_{Br}, δ_{Bt}, δ_S and δ_G represent the bending deformation of the rectangular portion, bending deformation of trapezoidal part, deformation produced by shear and the deformation caused by the sloping of the basic part, respectively, which can be represented by:

$$\begin{aligned}
\delta_{Br} &= \frac{12F_n\cos^2\omega_x}{EBs_F^3}\left(h_x h_r(h_x - h_r) + \frac{h_r^3}{3}\right) \\
\delta_{Bt} &= \frac{6F_n\cos^2\omega_x}{EBs_F^3}\left(\frac{h_i - h_x}{h_i - h_r}\left(4 - \frac{h_i - h_x}{h_i - h_r}\right) - 2\ln\frac{h_i - h_x}{h_i - h_r} - 3\right)(h_i - h_r)^3 \\
\delta_s &= \frac{2(1+\nu)F_n\cos^2\omega_x}{EBs_F}\left[h_r + (h_i - h_r)\ln\frac{h_i - h_r}{h_i - h_x}\right] \\
\delta_G &= \frac{24F_n h_x\cos^2\omega^2}{\pi EBs_F^2}
\end{aligned} \tag{2}$$

Here E, B and v refer to Young's modulus, face width and Poisson's ratio, respectively.

To conclude, the total deformation of meshing teeth along the direction of action can be expressed as:

$$\delta_\Sigma = \delta_1 + \delta_2 + \delta_p \tag{3}$$

where δ_1 and δ_2 are the deformation of each tooth, respectively, and δ_P refers to the deformation of the tooth contact segment (Li *et al.*, 2010), which can be described as:

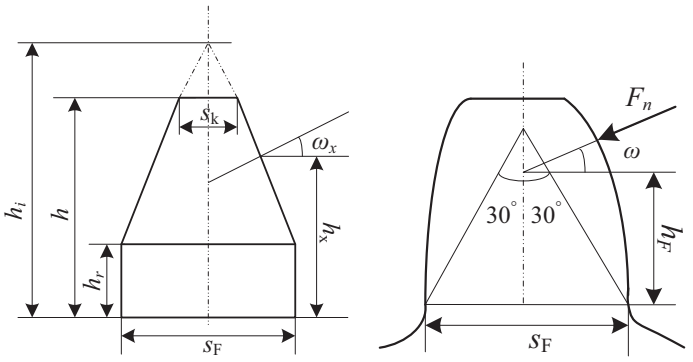

Figure 2.
The simplified model of gear tooth using Ishikawa method

$$\delta_p = \frac{4(1-v^2)F_n}{\pi EB} \tag{4}$$

Hence, the meshing stiffness of single tooth pair k_1(t) can be represented by:

$$k_1(t) = \frac{F_n}{\delta_\Sigma} \tag{5}$$

However, single and double teeth pair always mesh alternately in the actual meshing process. Apparently, the combination meshing stiffness of gear pair is made up of instantaneous meshing stiffness of each tooth pair involved in the meshing process, which is influenced by contact ratio.

In Figure 3, the meshing period t_m consists of double-tooth meshing period t_d and single-tooth meshing period t_s. In addition, ζ is defined as a proportionality coefficient, which can be represented by:

$$\zeta = \frac{t_d}{t_m} \tag{6}$$

The relationship between the proportionality coefficient ζ and contact ratio ε is:

$$\zeta = \varepsilon - 1 \tag{7}$$

Hence, the integrated time-varying meshing stiffness $k(t)$ of gear pair can be described as:

$$k(t) = \begin{cases} k_2(t) & 2t_d \\ k_1(t) & t_s \end{cases} \tag{8}$$

Where $k_2(t)$ is the meshing stiffness in the double teeth meshing area.

In equation (8), the formula contains the single and double teeth meshing stiffness during meshing progress, which is used to calculate the time-varying mesh stiffness. The gear system parameters and material characteristics are listed in Tables I and II. Through solving the above equations, the single and double meshing stiffness curves are presented in Figure 4, respectively. Thus, the time-varying mesh stiffness of the traction gear pair system is obtained in Figure 5.

During the meshing process, the comprehensive meshing stiffness exhibits a remarkable periodicity, which can be expanded by the way of Fourier series and then can be written with non-dimensional parameter as follows:

$$k(\tau) = \begin{cases} k_{2m} + \sum_{p=1}^{n} \left[a_{2p}\cos(p\omega\tau) + b_{2p}\sin(p\omega\tau) \right] & 0 < \tau \le 1.463\pi \\ k_{1m} + \sum_{q=1}^{n} \left[a_{1q}\cos(q\omega\tau) + b_{1q}\sin(q\omega\tau) \right] & 1.463\pi < \tau \le 2\pi \end{cases} \tag{9}$$

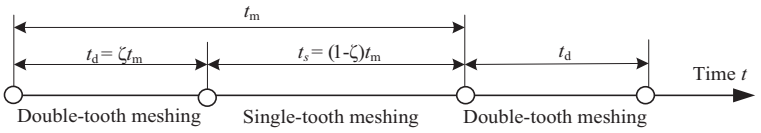

Figure 3.
Scheme of meshing period of tooth pair

Where $k_{2(1)m}$, $a_{2(1)}$ and $b_{2(1)}$ are the coefficient values of Fourier series, respectively. Here, only the first- and third-order Fourier series are considered, in which the corresponding coefficients are listed in Table III.

Then, the curve of gear meshing stiffness with three dimensionless meshing period is shown in Figure 6.

3.1.2 Validation of meshing stiffness. To verify the accuracy of the meshing stiffness, the result from the Ishikawa method will be compared with that from the energy method (Tian, 2004; Chen and Shao, 2011; Wan *et al.*, 2014). According to the energy method, the total potential energy U stored in gear system during meshing process includes five parts: Hertzian energy U_h, bending energy U_b, shear energy U_s, axial compressive energy U_a and gear fillet-foundation energy U_f, which can be expressed as follows:

$$U_h = \frac{F^2}{2k_h},\ U_b = \frac{F^2}{2k_b},\ U_s = \frac{F^2}{2k_s},\ U_a = \frac{F^2}{2k_a},\ U_f = \frac{F^2}{2k_f} \tag{10}$$

Table I.
Main parameters of the traction system of locomotive

Parameter	Driving/driven gear
Contact ratio ε	1.732
Transmission ratio	5.217
Number of teeth z_1/z_2	23/120
Radius of reference circle r (mm)	92/480
Module m (mm)	8
Pressure angle α (°)	20
Face width B (mm)	140
Driving torque T_1 (N·m)	5×10^3
Mass of wheel axle Q (N)	2.3×10^5
Wheel radius R (m)	0.625

Table II.
Material characteristics of gear

Parameter	Value
Material	18CrNiMo
Density ρ (kg·m^{-3})	7,870
Young's modulus E (Gpa)	207
Poisson's ratio v	0.26

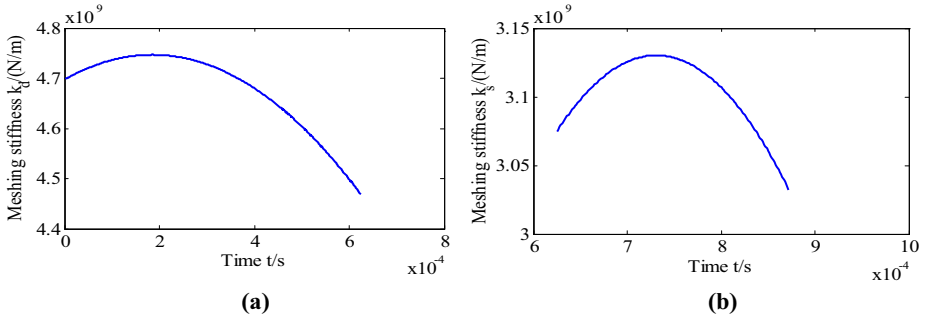

Figure 4.
The meshing stiffness curves under the double-tooth meshing period (a) and single-tooth meshing period (b), respectively

Where k_h, k_b, k_s, k_a and k_f refer to the Hertzian stiffness, bending stiffness, shear stiffness, axial compressive stiffness and gear fillet-foundation stiffness, respectively, and F is the load acting on the meshing point.

Therefore, the total potential energy U stored in a pair of meshing teeth can be written as:

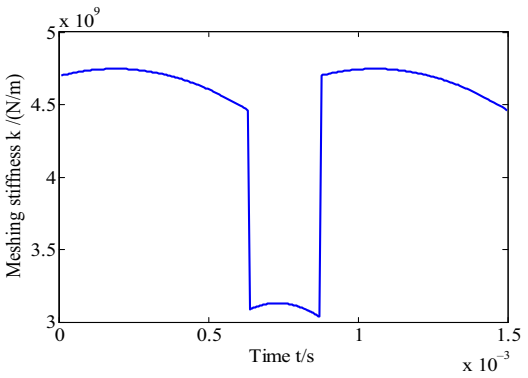

Figure 5.
The curve of time-varying meshing stiffness

Order	Coefficient
$k_{2(1)\,m}$	9.62×10^{-1} (6.56×10^{-1})
$a_{2(1)\,1}$	8.13×10^{-2} (3.91×10^{-2})
$b_{2(1)\,1}$	5.96×10^{-2} (9.1×10^{-3})
$a_{2(1)\,2}$	-2.8×10^{-3} (-3.8×10^{-3})
$b_{2(1)\,2}$	-1.35×10^{-2} (-1.2×10^{-3})
$a_{2(1)\,3}$	-9×10^{-4} (4×10^{-4})
$b_{2(1)\,3}$	1.3×10^{-3} (4×10^{-5})

Table III.
Coefficients of Fourier series

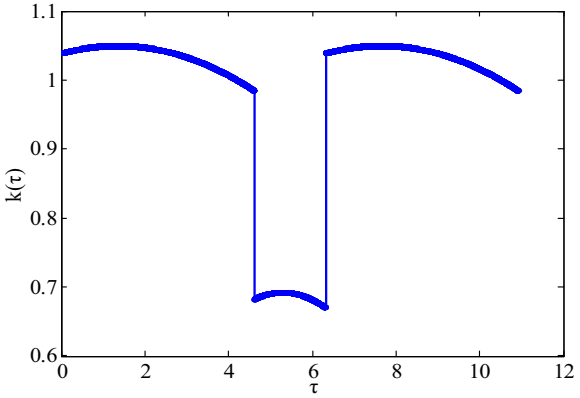

Figure 6.
The curve of gear meshing stiffness with dimensionless time from Ishikawa method

$$U = \frac{F^2}{2k_1} = U_h + U_{b1} + U_{s1} + U_{a1} + U_{f1} + U_{b2} + U_{s2} + U_{a2} + U_{f2} = \frac{F^2}{2}\left(\frac{1}{k_h} + \sum_{i=1}^{2}\left(\frac{1}{k_{bi}} + \frac{1}{k_{si}} + \frac{1}{k_{ai}} + \frac{1}{k_{fi}}\right)\right) \tag{11}$$

Where k_1 denotes the total stiffness in single teeth meshing area, which can be expressed as:

$$k_1 = \frac{1}{\frac{1}{k_h} + \sum_{i=1}^{2}\left(\frac{1}{k_{bi}} + \frac{1}{k_{si}} + \frac{1}{k_{ai}} + \frac{1}{k_{fi}}\right)} \tag{12}$$

Here i is equal to 1 or 2, which stands for driving or driven gear.

Because of the contact ratio, there exists the alternation meshing between the single tooth and double teeth, the time-varying mesh stiffness k_2 in the double teeth meshing area can thus, be expressed as:

$$k_2 = \sum_{j=1}^{2} \frac{1}{\frac{1}{k_h} + \sum_{i=1}^{2}\left(\frac{1}{k_{bi}} + \frac{1}{k_{si}} + \frac{1}{k_{ai}} + \frac{1}{k_{fi}}\right)} \tag{13}$$

Where j is 1 or 2, which refers to the j-th pair of meshing teeth.

Solving equations (12) and (13) from the energy method, thus the meshing stiffness can be obtained as shown in Figure 7. Meantime, Table IV presents the comparison of meshing stiffness error from two kinds of methods, where the relative error is less than 4 per cent. Therefore, the accuracy of the time-varying meshing stiffness based on the Ishikawa method is acceptable.

Blue line results from Ishikawa method and red line from energy method.

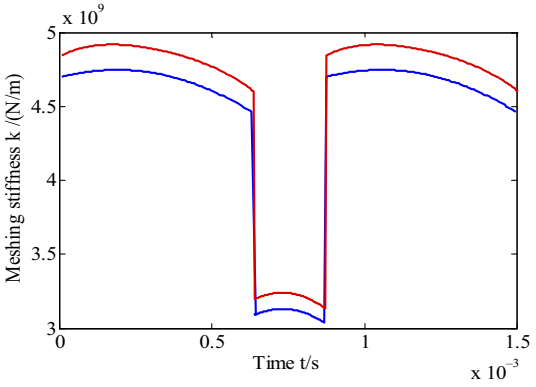

Figure 7.
The curve of gear meshing stiffness

3.2 Meshing transmission error

The meshing transmission error of gear pair is mainly caused by tooth manufacturing error and installation error. It makes the meshing tooth profile to deviate from the theoretical meshing position, destroying the correct meshing way of the involute gear and changing the instantaneous transmission ratio, which can result in the generation of the gear error excitation. Accordingly, the error excitation (Kahraman and Singh, 1991) can be expressed by harmonic functions:

$$e(t) = e_m + \sum_{r=1}^{\infty}(c_n \cos r\omega t + d_n \sin r\omega t) \tag{14}$$

Where e_{m} is the mean error. c_{n} and d_{n} are the expansion coefficient of the Fourier series. Only considering the first-order, the equation (14) can be simplified as (Xu *et al.*, 2013):

$$e(t) = e_m + e_a \cos(\omega t + \varphi) \tag{15}$$

Where e_m shows the average term, e_{a} represents the fluctuation and φ refers to the initial phase angle.

3.3 Gear backlash

In general, gear backlash is caused by gear lubrication and errors in manufacturing, as well as installation, which would make the meshing contact of gear pair change between contact and separation state. Hence, backlash should be considered in the system. Thus, the relative deformation $f(x)$ of the meshing teeth can be described as:

$$f(x) = \begin{cases} x - b & x > \mathrm{b} \\ 0 & |x| \le b \\ x + b & x < -\mathrm{b} \end{cases} \tag{16}$$

Where b refers to the half of gear backlash and x is the relative displacement of the teeth along the mesh line.

3.4 Friction excitation

Figure 8 shows the diagrammatic drawing of the meshing gear pair at the end surface. In Figure 8, r_{ai} and r_i (i = 1, 2) represent the radius of addendum and pitch circles, respectively. B_1 and B_2 are the departure and terminal points of the theoretical meshing line, respectively. A_1 and A_2 are the departure and terminal points of the actual meshing line, respectively. Meantime, l is the length of the actual meshing line. l_2 refers to the distance from pitch point P to ending point A_2 of the actual meshing line.

Item	Value from Ishikawa/energy method
Maximum stiffness in single teeth meshing (10^9 N/m)	3.128/3.238
Relative error (%)	3.497
Mean value of meshing stiffness (10^9 N/m)	4.314/4.480
Relative error (%)	3.847

Table IV. Comparison of meshing stiffness error

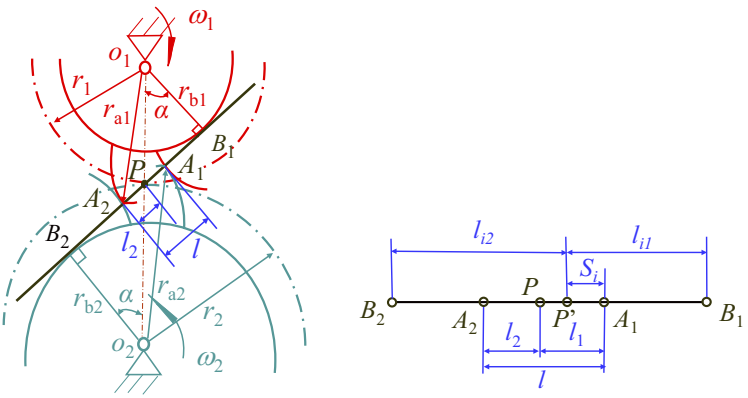

Figure 8.
Diagrammatic drawing of meshing gear pair at end plane

According to the geometric relationship between the two gears (Lu *et al.*, 2015), the physical parameters can be written as:

$$\begin{cases} l = \sqrt{r_{a1}^2 - r_{b1}^2} + \sqrt{r_{a2}^2 - r_{b2}^2} - (r_1 + r_2)\sin\alpha \\ l_2 = \sqrt{r_{a1}^2 - r_{b1}^2} - r_2\sin\alpha \\ l_{j1} = (r_1 + r_2)\sin\alpha - \sqrt{r_{a2}^2 - r_{b2}^2} + S_j \\ l_{j2} = \sqrt{r_{a2}^2 - r_{b2}^2} - S_j \end{cases} \tag{17}$$

Where l_{j1} and l_{j2} represent the frictional force arms of two gears. S_j is defined as the distance that the j-th pair of teeth ($j = 1, 2, \ldots, N$) moves path when entering into the meshing region during time t, which can be performed as:

$$S_j = \omega_1 r_{b1}\left[mod(t, t_m) + (j-1)t_m\right] \tag{18}$$

Here N stands for the maximum value of teeth involved in meshing at the same time and can be obtained as:

$$N = ceil(\varepsilon) \tag{19}$$

During meshing process of gears, the meshing point moves along the meshing line, where the instantaneous radius of curvature at the contact point, the relative sliding velocity of contact surface of two teeth, and contact load are all changing, leading to the variation of the magnitude and direction of friction force. Accordingly, the friction force can be given by:

$$F_f = \sum_{j=1}^{N} F_{fj} = \sum_{j=1}^{N} \lambda_j \mu_B F_j \tag{20}$$

Here λ_j refers to the direction coefficient of friction force, μ_B stands for the coefficient of sliding friction and F_j represents meshing force, which can be expressed as:

$$F_j = k_j(t) \cdot f(x) + c_m \cdot \frac{dx}{dt} \tag{21}$$

The coefficient of sliding friction μ_B is calculated using Buckingham semi-empirical formula (Qin *et al.*, 2015), which can be described as:

$$\mu_B = 0.05e^{-0.003175v_s} + 3.187 \times \sqrt{v_s} \tag{22}$$

Where v_s is the relative slip velocity between gears.

Additionally, the direction coefficient of friction force λ_j adopts the following expression:

$$\lambda_j = \begin{cases} 1 & 0 < S_j < l_1 \\ 0 & l < S_j < NP_t \\ -1 & l_1 < S_j < l \end{cases} \tag{23}$$

Then, the friction moments of two gears can be obtained as:

$$\begin{cases} T_{f1} = \sum_{j=1}^{N} T_{fj1} = \sum_{j=1}^{N} F_{fi} \cdot l_{j1} \\ T_{f2} = \sum_{j=1}^{N} T_{fj2} = \sum_{j=1}^{N} F_{fj} \cdot l_{j2} \end{cases} \tag{24}$$

4. External excitation

During running, the locomotive is driven by the adhesion force generated between wheelset and rail. As a result, the adhesion-slip feature between wheelset and rail has a direct influence on the driving and braking performance of the locomotive. Because of the relative sliding of wheel/rail resulting in friction force, the adhesion phenomenon occurs. In other words, when the relative sliding happens, the instantaneous velocity of the locomotive is not equal to the linear speed of wheelset. Thus, creep ratio s is introduced to describe the sliding state, which is defined as follows:

$$s = \frac{\omega R - v_L}{\omega R} \tag{25}$$

Where R refers to the radius of the wheel, ω represents the instantaneous angular velocity of the wheel and v_L is the driving speed of the locomotive.

When the relative movement between wheel and rail appears, the contact condition is always composed of the adhesion zone and slip zone, as shown in Figure 9. As creep ratio s is zero, the wheelset is completely in the adhesion zone, which indicates that the wheelset runs by the way of pure rolling, as seen in Figure 9(a). Later, with the increase of s slightly, the adhesion zone is reduced a bit and the sliding zone is increased. However, the adhesive

zone is still the main contact area, as seen in Figure 9(b). Subsequently, with the change of s continuously, the slip zone becomes the main contact area, in which the adhesion force keeps increasing as s increases. Then, the adhesion force reaches the maximum when s increases to the critical value that makes the contact area becomes the whole slip zone, as shown in Figure 9(d). The slippage process can be revealed by the polyline O-A-B-C from Figure 10.

However, the actual research (Yao *et al.*, 2011) represents that the adhesion force decrease gradually when the creep ratio increases further from the critical value, as the wheel-rail friction heat and rail surface roughness increase. The phenomenon can be observed from the polyline O-A-B-D in Figure 10. Based on the actual condition, the adhesion coefficient curve between wheel and rail is simplified as seen in Figure 11. For analytical convenience, the simplified adhesion coefficient curve in Figure 11 is divided into two parts. The condition that the creep ratio lies in the region of $s < s_{\mathrm{m}}$ is seen as Case I. The other range of creep ratio is defined as Case II. Thus, the simplified adhesion coefficient curve can be described by the following function:

$$\mu = \begin{cases} \mu_{\mathrm{m}} s / s_m & \text{Case I} \\ \mu_{\mathrm{m}} + k_\mu (s - s_m) & \text{Case II} \end{cases} \tag{26}$$

Where μ_{m} refers to the maximum adhesion coefficient and s_{m} is the critical creep rate corresponding to μ_{m}. In addition, k_μ is the negative slope of the adhesion curve.

Therefore, the adhesion force F_{w} and load torque T_2 can be represented by:

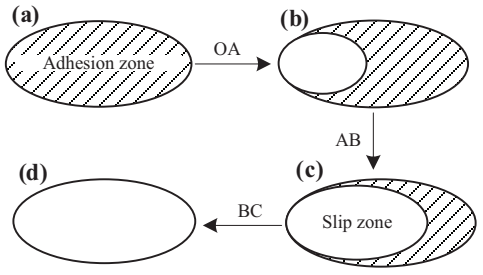

Figure 9.
Sketch of contact condition between wheel and rail including pure adhesion zone (a), coexistence zone of adhesion (b) and slip (c), and pure slip zone (d)

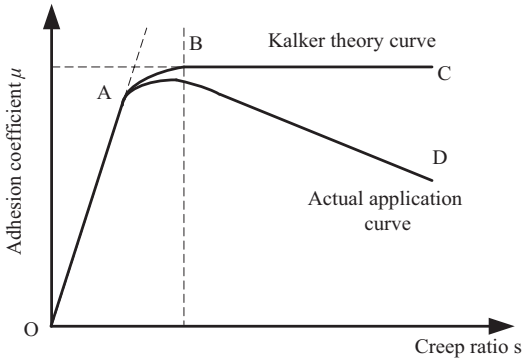

Figure 10.
Adhesion coefficient curve between wheel and rail

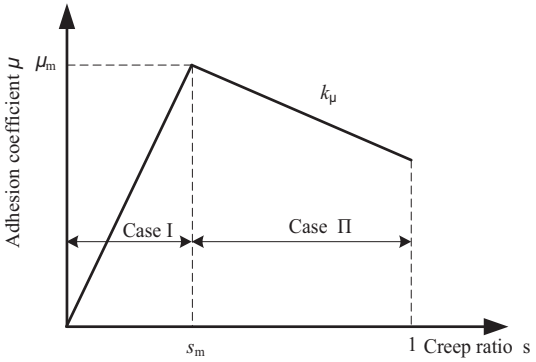

Figure 11.
Simplified adhesion coefficient curve

$$\begin{aligned} F_{\mathrm{w}} &= \mu Q \\ T_2 &= F_w R \end{aligned} \tag{27}$$

Where Q represents the axle load of the wheelset.

Substituting equation (26) into equation (27), the load torque T_2 can be transformed into the following expressions:

$$T_2 = \begin{cases} \mu_{\mathrm{m}} RQs/s_m & \text{Case I} \\ \mu_{\mathrm{m}} RQ + RQk_\mu (s - s_m) & \text{Case II} \end{cases} \tag{28}$$

5. Equations of motion

Figure 1 presents the simplified torsional lumped parameter model of the traction system. Thus, the differential equations of motion of the system can be described as follows:

$$\begin{cases} I_1 \dfrac{d^2\theta_1}{dt^2} = T_1 - r_{b1} \displaystyle\sum_{j=1}^{N} F_j - T_{f1} \\ I_2 \dfrac{d^2\theta_2}{dt^2} = -T_2 + r_{b2} \displaystyle\sum_{j=1}^{N} F_j + T_{f2} \end{cases} \tag{29}$$

The relative displacement x along the meshing line with $x = r_{b1}\theta_1 - r_{b2}\theta_2 - e(t)$ is introduced, so that the equation (29) can then be expressed as:

$$\begin{aligned} &\frac{d^2x}{dt^2} + \left(\frac{1}{m_{e1}} + \frac{1}{m_{e2}}\right) \sum_{j=1}^{N} F_j + \left(\frac{1}{r_{b1}m_{e1}} T_{f1} + \frac{1}{r_{b2}m_{e2}} T_{f2}\right) \\ &\quad = \frac{1}{r_{b1}m_{e1}} T_1 + \frac{1}{r_{b2}m_{e2}} T_2 - \frac{d^2e(t)}{dt^2} \end{aligned} \tag{30}$$

Where $m_{e1} = I_1/r_{b1}^2$ and $m_{e2} = I_2/r_{b2}^2$.

Substituting equations (20), (24) and (28) into equation (30), the equation (30) can be rewritten as:

$$\frac{d^2x}{dt^2}+\frac{1}{m_e}\left(c_m\cdot H_1(t)+c_m\cdot H_2(t)\right)\frac{dx}{dt}+\frac{1}{m_e}\left(k_1(t)\cdot H_1(t)+k_2(t)\cdot H_2(t)\right)\cdot f(x)$$
$$=\begin{cases}\dfrac{F_1}{m_{e1}}+\dfrac{\mu_m RQs}{m_{e2}s_m}-\dfrac{d^2e(t)}{dt^2} & s<s_{\mathrm{m}}\\ \dfrac{F_1}{m_{e1}}+\dfrac{1}{m_{e2}}\left(\mu_m RQ+RQk_\mu(s-s_m)\right)-\dfrac{d^2e(t)}{dt^2} & s_{\mathrm{m}}<s<1\end{cases} \tag{31}$$

Where

$$m_{\mathrm{e}}=\frac{m_{\mathrm{e1}}m_{\mathrm{e2}}}{m_{\mathrm{e1}}+m_{\mathrm{e2}}}\quad H_1(t)=1+\lambda_1\mu_B m_{\mathrm{e}}\left(\frac{l_{11}}{r_{b1}m_{\mathrm{e1}}}+\frac{l_{12}}{r_{b2}m_{\mathrm{e2}}}\right)$$

$$H_2(t)=1+\lambda_2\mu_B m_{\mathrm{e}}\left(\frac{l_{21}}{r_{b1}m_{\mathrm{e1}}}+\frac{l_{22}}{r_{b2}m_{\mathrm{e2}}}\right)$$

Subsequently, the two dimensionless symbol τ with $\tau=\omega_{\mathrm{n}}t$ and b_{c} are introduced as well, where $\omega_{\mathrm{n}}=\sqrt{k_{\mathrm{m}}/m_{\mathrm{e}}}$ is the natural frequency. The dimensionless displacement, velocity and acceleration of the system can be expressed, respectively, as follows: $x=Xb_c$, $\frac{dx}{dt}=\frac{dX}{dt}b_c\omega_n$, $\frac{d^2x}{dt^2}=\frac{d^2X}{dt^2}b_c\omega_n^2$ and $\Omega=\omega/\omega_{\mathrm{n}}$. Therefore, equation (31) can be represented in the dimensionless form:

$$\frac{d^2X}{dt^2}+2\xi\left(H_1(\tau)+H_2(\tau)\right)\frac{dX}{dt}+\frac{1}{k_m}\left(k_1(\tau)H_1(\tau)+k_2(\tau)H_2(\tau)\right)f(X)$$
$$=\begin{cases}\dfrac{F_1}{b_cm_{e1}\omega_n^2}+\dfrac{\mu_m RQs}{b_cm_{e2}\omega_n^2s_m}-F_a\Omega^2\cos(\Omega\tau) & s<s_{\mathrm{m}}\\ \dfrac{F_1}{b_cm_{e1}\omega_n^2}+\dfrac{1}{b_cm_{e2}\omega_n^2}\left(\mu_m RQ+RQk_\mu(s-s_m)\right)-F_a\Omega^2\cos(\Omega\tau) & s_{\mathrm{m}}<s<1\end{cases} \tag{32}$$

where

$$\xi=\frac{c_m}{2m_e\omega_n}\quad F_a=e_a/b_c\quad f(X)=\begin{cases}X-D & X>D\\ 0 & |X|\le D\\ X+D & X<-D\end{cases}$$

6. System response and discussions

To control the motion response and improve the running stability of the locomotive traction gear pair system, it is extremely indispensable to understand comprehensively the dynamic characteristic of the system.

In this section, exciting frequency Ω, load torque T_2, gear backlash D, error fluctuation F_a and friction coefficient u_B are chosen to be the control parameters to analyze the influences on the dynamic behaviors of the traction system. Meanwhile, to identify and discuss exactly the dynamic responses of the system, bifurcation diagram, time history, three-dimensional frequency spectrum, phase portrait, spectrum plot and Poincaré map are presented. A case study about a kind of locomotive is introduced to analyze, in which the main system parameters are listed in Table I.

6.1 Effect of exciting frequency and load torque on dynamic response

In the subsection, a detailed study is performed to reveal the influence of exciting frequency Ω and load torque T_2 on the dynamic response. As the main external excitation, load torque T_2 is the paramount factor that can affect the dynamic characteristic of the traction system. Owing to the piecewise trait of load torque, which can be verified from equation (28), the dynamic feature of the driving system would be analyzed under Cases I and II, respectively. Keeping other system parameters constant, Figures 12(a) and 12(b) present the bifurcation diagrams of the traction system with dimensionless exciting frequency Ω varying under Cases I and II, respectively. Meanwhile, to clearly determine the frequency component of motion state for the system, the corresponding three-dimensional frequency spectrums are demonstrated in Figures 13(a) and 13(b). In these figures, the exciting frequency Ω is under the range of 0-2.5, where the corresponding rotational speed of driving gear changes from 0 to 2,250 r/min.

As seen in Figures 12(a) and 12(b), the bifurcation characteristics of exciting frequency Ω versus displacement X show obvious difference under Cases I and II. From Figure 12(a), in

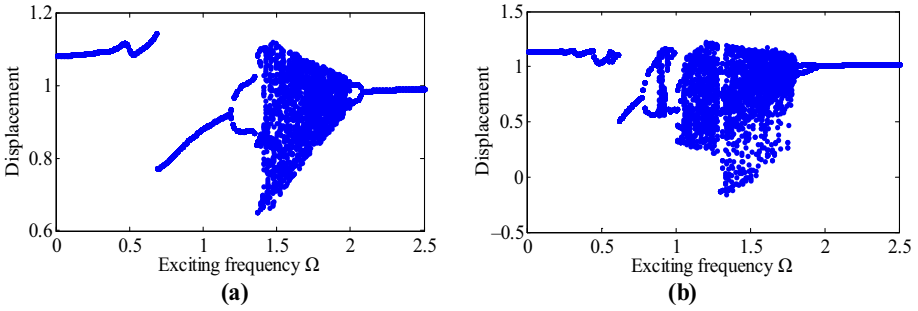

Figure 12. Bifurcation diagrams of exciting frequency Ω versus displacement under Case I (a) and under Case II (b)

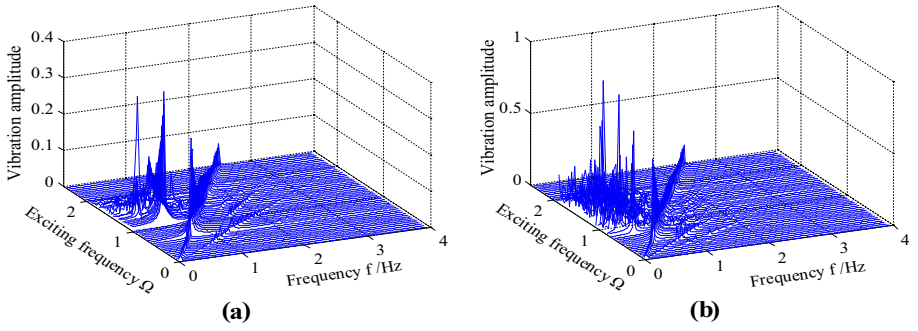

Figure 13. Three-dimensional frequency spectrums of the traction system under Case I (a) and Case II (b)

the range of exciting frequency $\Omega < 1.18$, the system gets into p-1 (periodic-one) motion, where the jump discontinuous phenomenon appears at $\Omega = 0.68$. Further increasing Ω, the system turns into p-2 motion. Then, the system response transits to chaotic behavior. When Ω increases even further, the motion form changes from chaos to p-2 state. Finally, the system reverts to p-1 motion. However, the dynamic responses of the traction system become rich and complex under Case II, which can be observed from Figure 12(b). At low values of exciting frequency, namely, $\Omega < 0.54$, the system is also under p-1 motion. As Ω increases, it gets into a narrow window of p-2 state. Then, the motion returns once again to the p-1 motion. Similarly, there is a crisis phenomenon at $\Omega = 0.62$ during p-1 motion, which is similar under Case I. When Ω changes further, the system turns into p-2 motion, which can be shown in Figure 14 with $\Omega = 0.78$. From the figure, it shows that phase diagram has two sealed circles and there are also two individual points in the Poincaré map. These results signify that the system is under p-2 motion. As Ω increases to 0.83, the system response is p-4 motion in Figure 15. With Ω keeps increasing, the system transits to a chaotic state. As an example, when Ω is equal to 0.9, the time history concerning displacement is irregular, spectrum plot possesses a multitude of different and continuous frequency components, the phase diagram demonstrates disorder pattern and a number of discrete points appear in Poincaré map, as illustrated in Figures 16(a)-16(d). These features reveal the system is in an unstable state. After undergoing the brief process of chaos, the system switches to period motion. For instance, at $\Omega = 0.93$, the wave of vibration displacement shows the period motion, phase diagram is composed of several closed circles and Poincaré map consists of seven discrete points in Figure 17, which indicates the system response is in multi-period motion. The system then transfers into chaos again, which can be shown in Figure 18. Finally, the dynamic behavior of the system is found to be p-2 and p-1 motions.

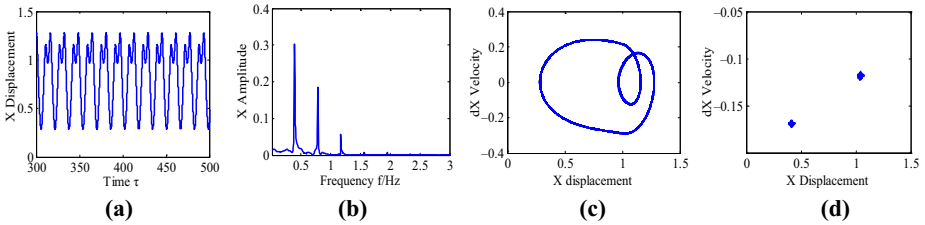

Figure 14.
System response at $\Omega = 0.78$

Notes: (a) Time history; (b) spectrum plot; (c) phase portrait; (d) poincaré map

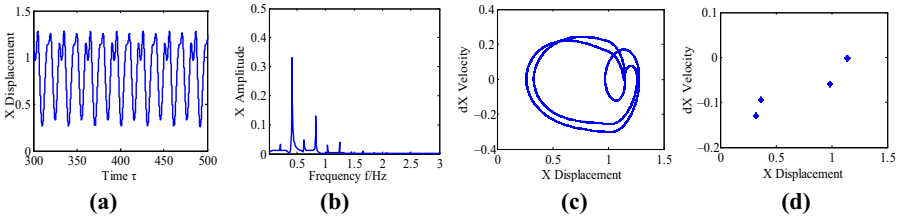

Figure 15.
System response at $\Omega = 0.83$

Notes: (a) Time history; (b) spectrum plot; (c) phase portrait; (d) poincaré map

From Figures 13(a) and 13(b), it could be observed that the frequency components in Figure 13(b) are more complex than those in Figure 13(a). In the range of $0 < \Omega < 1$, there exist two types of main frequency components in Figure 13(a), namely, Ω and 0.5Ω. However, the continuous and intricate frequency components appear sometimes under $\Omega < 1$ in Figure 13(b), which can be seen in Figure 16(b) at $\Omega = 0.9$. Similarly, the width of window that the complex and disordered frequency component would occur is wider when Ω is under the region (1, 2) in Figure 16(b) than that in Figure 16(a), which can be identified from the corresponding bifurcation diagrams in Figure 12 as well.

The above results have shown that the transition process of motion states of the system is more complicated under Case II, especially where the window of chaotic motion become wider. Under chaotic motion, the system becomes invariably unpredictable and uncontrollable. Therefore, to avoid complex dynamic behaviors of system appear and keep locomotive running stably, the load torque T_2 should be less than the critical value. In other words, the value of adhesion coefficient should be chosen with the range of $0 < s < s_m$, which can prevent the self-excited vibration of traction system (Yao *et al.*, 2015).

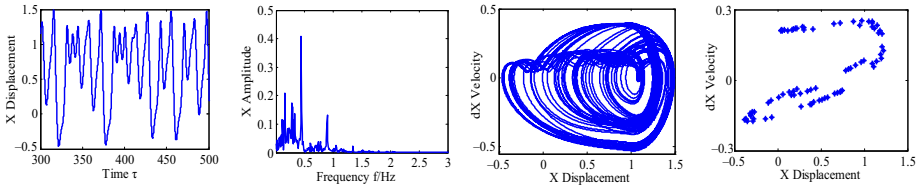

Figure 16. System response at $\Omega = 0.9$

Notes: (a) Time history; (b) spectrum plot; (c) phase portrait; (d) poincaré map

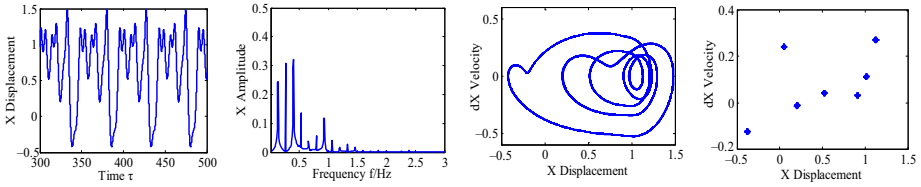

Figure 17. System response at $\Omega = 0.93$

Notes: (a) Time history; (b) spectrum plot; (c) phase portrait; (d) poincaré map

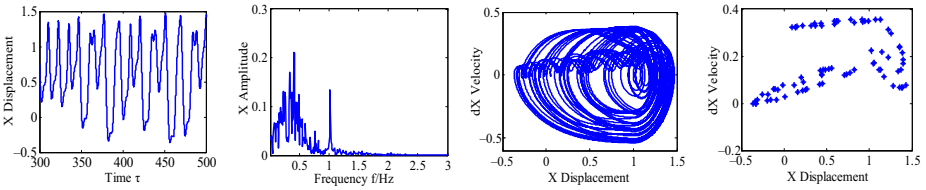

Figure 18. System response at $\Omega = 1.02$

Notes: (a) Time history; (b) spectrum plot; (c) phase portrait; (d) poincaré map

6.2 Effect of gear backlash on dynamic response

Because of manufacturing accuracy, installation error, thermal expansion of gear teeth and the request of gear lubrication, gear backlash always exists in the traction gear pair system, which can aggravate the degree of non-linear characteristic of system. Thus, gear backlash has an important impact on the system behavior. With the purpose of examining the influence of gear backlash on the system response, a particular analysis is performed, in which the bifurcation diagram of gear backlash D as control system under Case I is obtained in Figure 19(a). Meantime, the corresponding three-dimensional frequency spectrum is shown in Figure 19(b) to exhibit the frequency component with the change of gear backlash.

From Figure 19(a), it can be clearly noted that the system would go through a complex evolution process of motion states including single periodic, multi-periodic and chaotic motions as gear backlash D changes. At low values of D, the system undergoes p-1 motion, which can be found in Figure 20. In Figures 20(a) and 20(b), at $D = 0.1$, these display that time history of displacement is a sine curve and spectrum plot only contains two types of frequency components. Besides, there is a closed circle in the phase diagram and a single point appears in Poincaré graph as observed in Figures 20(c) and 20(d), which manifest the system is under p-1 motion. As D continues to increase, the motion response changes to p-2 state. Then, when D reaches to 0.15, the system enters into the chaotic state, where there appears complex and continuous harmonic components near 0.5Ω in spectrum plot and the fractal structure composed by numerous discrete points exists in Poincaré map as illustrated in Figures 21(b)-21(d). Before going into the next window of chaos, a short window of p-4 motion is observed. Choosing $D = 0.18$, the corresponding dynamic response can be seen in Figure 22, which can obviously determine that the system is at p-4 state. When D further

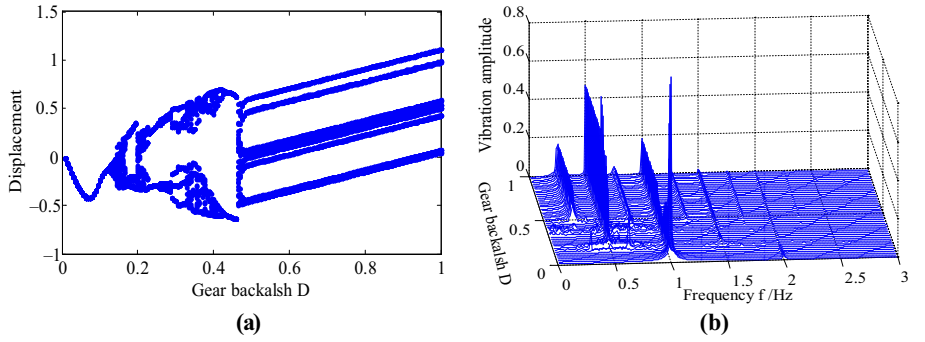

Figure 19. Bifurcation diagram (a) and three-dimensional frequency spectrum (b) of gear backlash D as a control system under case I

Notes: (a) Bifurcation diagram; (b) three-dimensional frequency spectrum

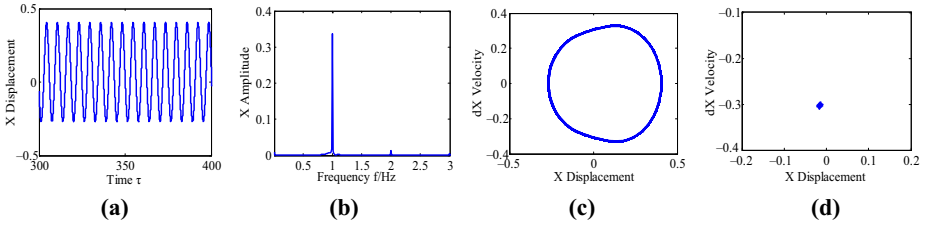

Figure 20. System response at $D = 0.1$

Notes: (a) Time history; (b) spectrum plot; (c) phase portrait; (d) poincaré map

increases to 0.21, the system gets into the chaos again as shown in Figure 23, where the dynamic response is similar to the result in Figure 21. As D keeps increasing, the response motion enters into multi-period state. Specifically, after the chaotic motion, the system first goes into p-4 state, then switches to p-2 and further returns into p-4, finally, transits to p-6 motion at $D = 0.30$ in Figure 24. With the increasing of D even further, the system response is transited from period motion to chaos, as shown in Figure 25. Finally, the system is always under period motions, which can be found in Figures 26 and 27.

In Figure 19(b), three-dimensional frequency spectrum shows intuitively the change of the frequency components of the system with gear backlash D varying. As $D < 0.25$, the meshing frequency Ω is dominated response, as illustrated in Figures 20(b)-24(b). In the range of $D < 0.45$, the system would undergo three window region of chaos, where there are continuous frequency components as shown in Figures 21(b), 23(b) and 25(b). In addition, when $D > 0.45$, the multiplication frequency and de-multiplication frequency components appear in spectrum plot, in which the phenomenon can be seen in Figure 27(b) as $D = 0.8$.

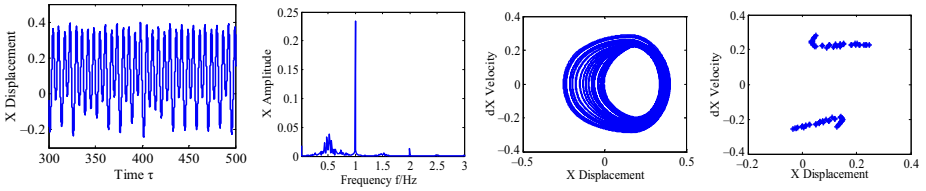

Figure 21. System response at $D = 0.15$

Notes: (a) Time history; (b) spectrum plot; (c) phase portrait; (d) poincaré map

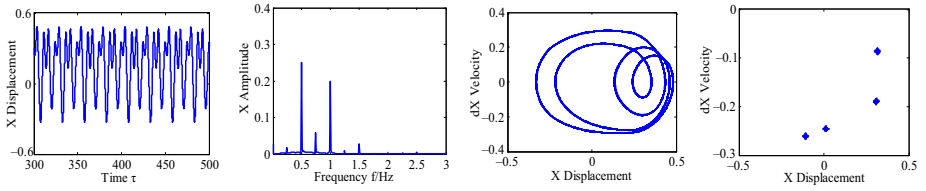

Figure 22. System response at $D = 0.18$

Notes: (a) Time history; (b) spectrum plot; (c) phase portrait; (d) poincaré map

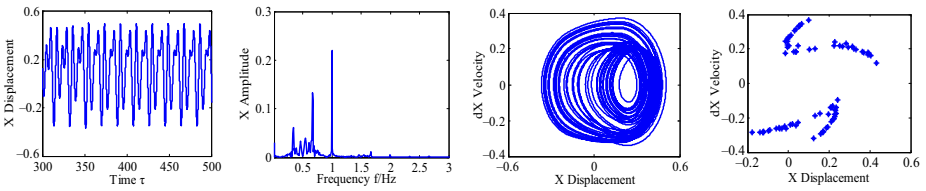

Figure 23. System response at $D = 0.21$

Notes: (a) Time history; (b) spectrum plot; (c) phase portrait; (d) poincaré map

According to the above analysis, the varying gear backlash D can give rise to rich bifurcation characteristics. However, under chaotic motion, the system becomes unstable and unpredictable. Herein, gear backlash should be selected adequately to make the system stable, where the above results could furnish the theoretical basis (Figures 23-27).

6.3 Effect of error fluctuation on dynamic response

As a displacement excitation, the transmission error is triggered by manufacturing error and installation error during meshing, which can impact the dynamic characteristics of the traction system. To demonstrate the point, a case study is analyzed where the error fluctuation F_a is used as the control parameter and the others keep a constant value. Herein, the bifurcation diagram and the corresponding three-dimensional frequency spectrum as F_a varies are shown under Case I in Figure 28.

As illustrated in Figure 28(a), the bifurcation features of the system are changed with the increasing error fluctuation F_a. When F_a is at a low value, the motion state of the system is

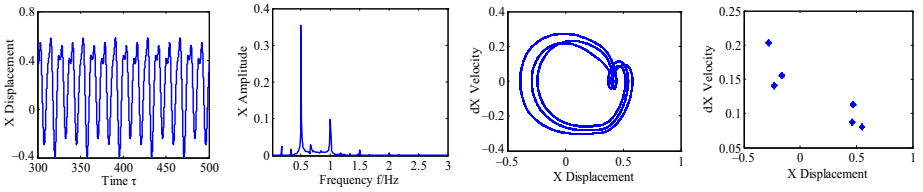

Figure 24.
System response at $D = 0.30$

Notes: (a) Time history; (b) spectrum plot; (c) phase portrait; (d) poincaré map

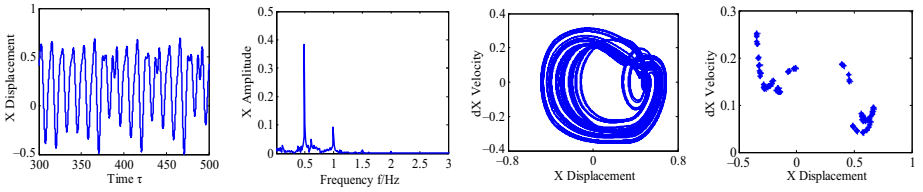

Figure 25.
System response at $D = 0.34$

Notes: (a) Time history; (b) spectrum plot; (c) phase portrait; (d) poincaré map

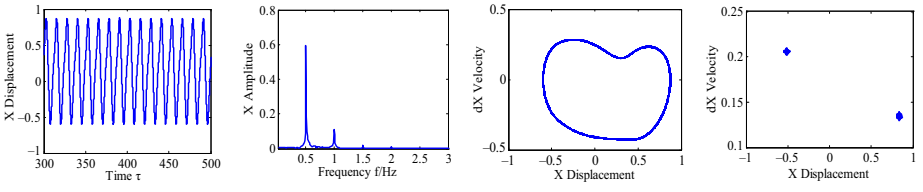

Figure 26.
System response at $D = 0.44$

Notes: (a) Time history; (b) spectrum plot; (c) phase portrait; (d) poincaré map

period motion. Choosing F_a = 0.12, the dynamic behavior is presented in Figure 29. The time-domain wave is a periodic curve, spectrum plot has three obvious amplitudes, phase diagram possess two closed circle and there are two points in Poincaré map, which clearly demonstrate the system is in p-2 motion. Keeping F_a increasing, it gets into the chaos state, as observed in Figure 30, in which there appears a disorder in phase diagram and numerous discrete points exit in the Poincaré map. However, when F_a reaches 0.27, the wave in Figure 31(a) shows a regular curve, the meshing frequency is dominated response in Figure 31(b), the phase diagram in Figure 31(c) shows disorder pattern, and there exist four points in the Poincaré map in Figure 31(d), indicating the system is under p-4 motion. Then, as F_a increases further, the system response becomes chaotic again. When F_a is equal to 0.3,

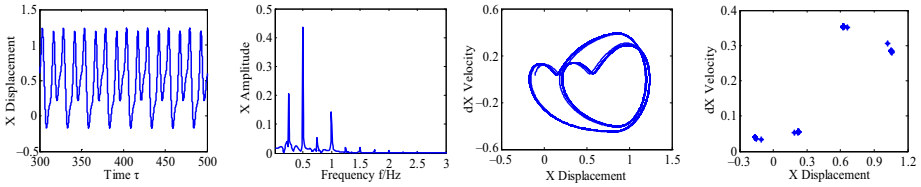

Figure 27. System response at D = 0.8

Notes: (a) Time history; (b) spectrum plot; (c) phase portrait; (d) poincaré map

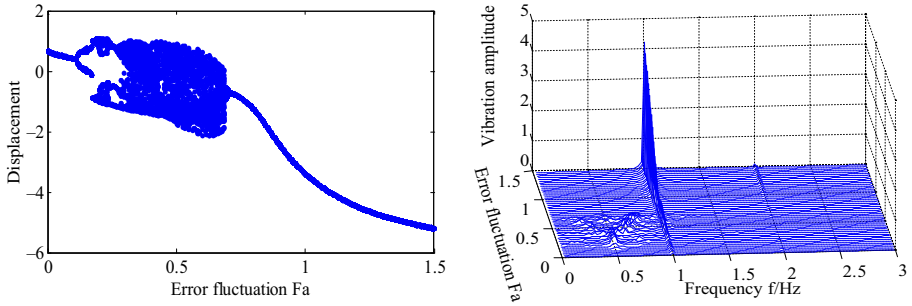

Figure 28. Bifurcation diagram (a) and three-dimensional frequency spectrum (b) of error fluctuation F_a as control system under Case I

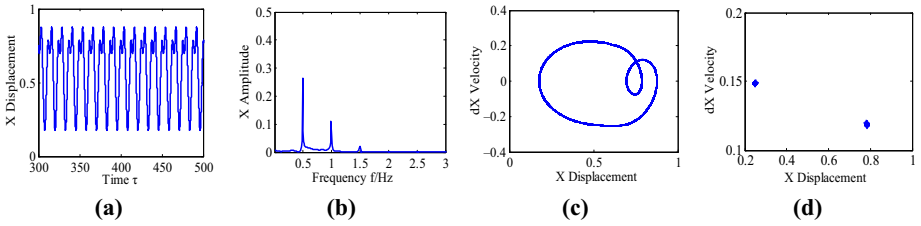

Figure 29. System response at Fa = 0.12

Notes: (a) Time history; (b) spectrum plot; (c) phase portrait; (d) poincaré map

the dynamic response in Figure 32 verifies the motion form of the system. Finally, the system returns to period motion. For instance, at F_a=0.70, it is under p-2 motion, which can be observed in Figure 33. Although always under the p-1 motion with the increasing of F_a even further, the amplitude of displacement of the system increases significantly as well. In

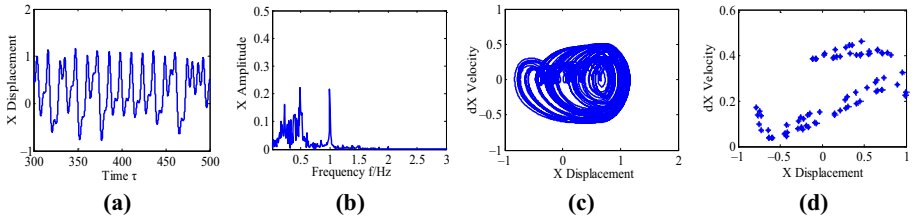

Figure 30.
System response at $Fa = 0.2$

Notes: (a) Time history; (b) spectrum plot; (c) phase portrait; (d) poincaré map

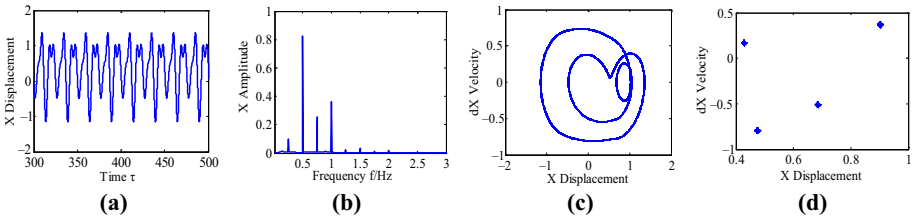

Figure 31.
System response at $Fa = 0.27$

Notes: (a) Time history; (b) spectrum plot; (c) phase portrait; (d) poincaré map

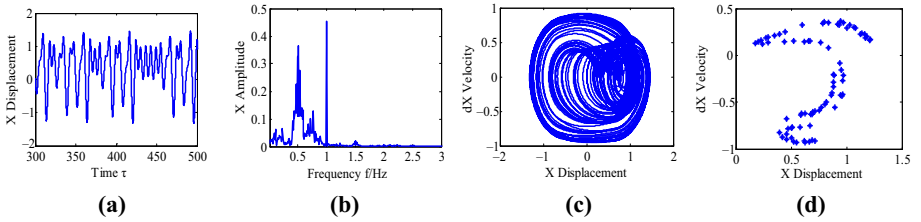

Figure 32.
System response at $Fa = 0.3$

Notes: (a) Time history; (b) spectrum plot; (c) phase portrait; (d) poincaré map

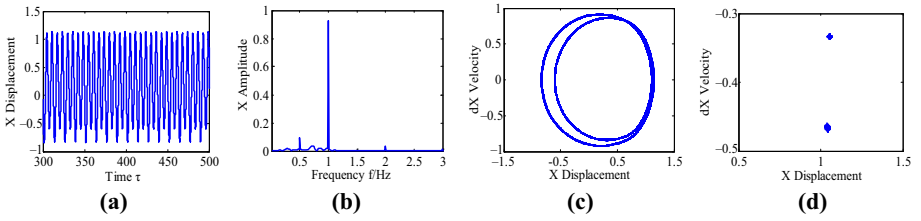

Figure 33.
System response at $Fa = 0.7$

Notes: (a) Time history; (b) spectrum plot; (c) phase portrait; (d) poincaré map

Figure 28(b), at low values of *F*a, the response peak appears in fractional frequency, namely, 0.5Ω. With the increase of F_a, the exciting frequency becomes the dominated response frequency, where the amplitude at Ω increases as well.

These above analysis results show that error fluctuation F_a can affect directly the motion state of the traction system. Accordingly, the value of F_a should be set reasonably to avoid chaos motion or/and large vibration amplitude.

6.4 Effect of friction coefficient on dynamic response

Considering the sliding friction force, the dynamics responses of traction gear pair system would show the different features than those without friction. To analyze the vibration response of traction system with or without friction force, the friction coefficient u_B is chosen as the control parameter. Keep other parameters be constant, the bifurcation diagram of the system with u_B varying in the range [0, 0.1] is indicated in Figure 34(a) based on the built model, while the bifurcation diagram in Figure 34(b) is obtained according to the method from reference (Wang *et al.*, 2017). With the increase of u_B, the gear pair system exhibits periodic-*n* and chaotic motions state, and the system displacement decrease gradually, which can be observed from Figure 34(a). Meantime, Figure 34(b) presents a similar variation tendency of displacement, while there shows different bifurcation characteristics owing to the friction force formula without consideration of the direction coefficient.

To show further the dynamic response of the system considering the effect of friction, Figures 35(a), 12(a) and 35(b) depict the bifurcation diagrams with exciting

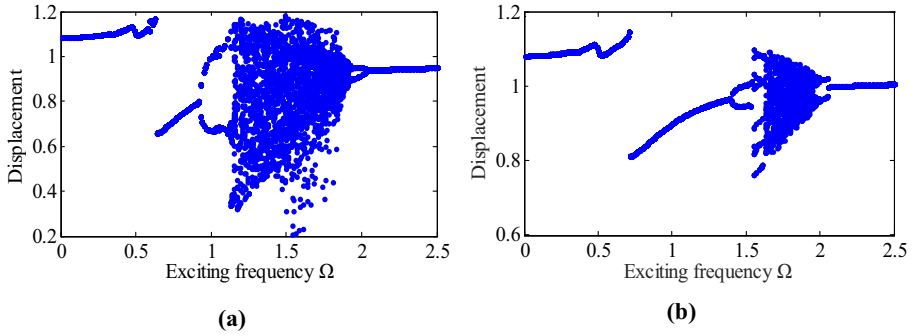

Figure 35. Bifurcation diagrams of exciting frequency Ω versus displacement with friction coefficient $u_B = 0$ (a) and $u_B = 0.1$ (b)

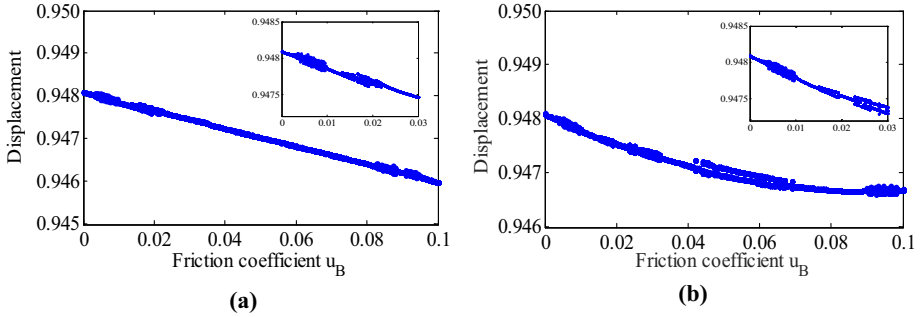

Figure 34. Bifurcation diagrams of friction coefficient u_B versus displacement by the method in the study (a) and the reference (Wang *et al.*, 2017) (b), respectively

frequency varying under different friction coefficient, namely, u_B = 0, 0.03 and 0.1, respectively. The corresponding three-dimensional frequency spectrums are shown in Figures 36(a), 13(a) and 36(b). As seen in the three bifurcation diagrams, the width of window of chaotic motion become narrow as u_B increases, which means system with friction trends to be stable. It can be verified from the corresponding three-dimensional frequency spectrums that the region of disordered frequency component reduces and the maximum vibration amplitude decrease as u_B increases.

Under different friction coefficient, the system response with the same exciting frequency can show different motion forms. When exciting frequency Ω is equal to initial value, the system with friction coefficient u_B = 0 (blue line) or u_B = 0.1 (red line) is in p-1 motion as shown in Figure 37. However, the response amplitude without friction is slightly larger than that with friction coefficient u_B = 0.1. As Ω increases, the system without friction enters into p-2 motion earlier as shown in Figure 38. For instance, at Ω = 1, there exists two discrete blue points and a discrete red point in Poincaré map of Figure 38(d), which indicates the system with friction or with friction coefficient u_B = 0.1 is under p-2 or p-1 motion, respectively. Meantime, the vibration amplitude with friction is obviously greater than that with friction. Then, with increase of Ω from 1.15 to 1.91, the system response without friction changes to chaotic motion, while the system with friction undergoes complex motion transformation including p-1, p-n and chaotic motions. For example, the system with friction starts with p-1 motion and then

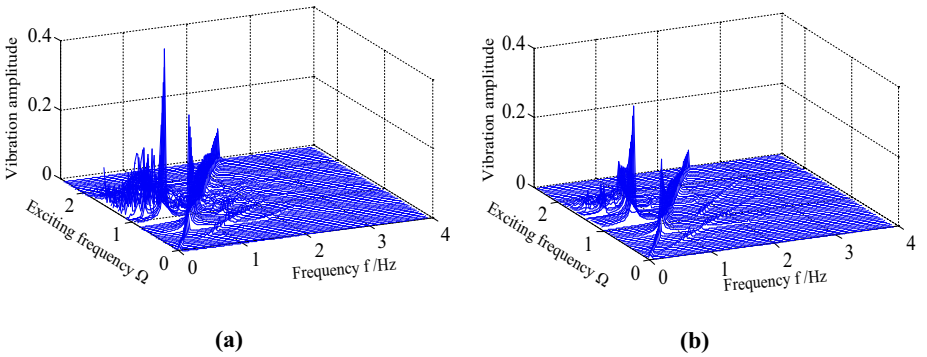

Figure 36.
Three-dimensional frequency spectrums of the traction system with friction coefficient u_B = 0 (a) and u_B = 0.1 (b)

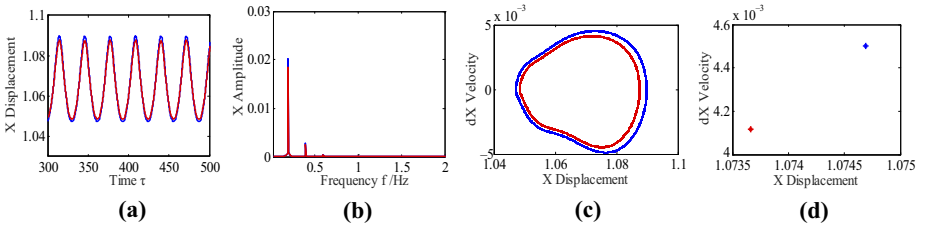

Figure 37.
System response at Ω = 0.2

Notes: (a) Time history; (b) spectrum plot; (c) phase portrait; (d) poincaré map

transits to p-2 motion in Figure 39 and p-8 motion in Figure 40 and further goes through the chaotic state in Figure 41, and finally, reduces to p-2 or p-1 motion. Certainly, the system without friction or with friction reverts to p-1 motion at last, as shown in Figure 42. According to the analysis above, the sliding friction has an important effect on the dynamic response of traction system, which can suppress the vibration amplitude and control unstable state of system.

7. Conclusions

This study presents a simulation model for locomotive traction gear system subjected to internal and external excitations such as backlash, time-varying meshing stiffness,

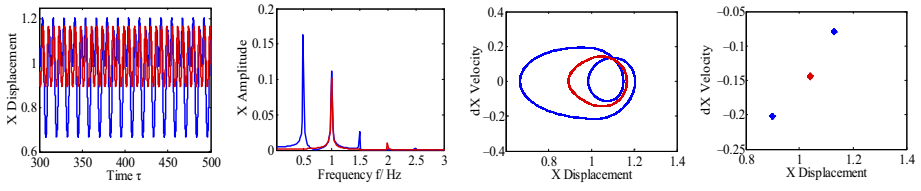

Figure 38. System response at $\Omega = 1$

Notes: (a) Time history; (b) spectrum plot; (c) phase portrait; (d) poincaré map

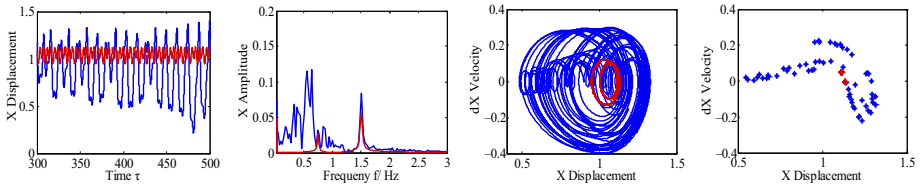

Figure 39. System response at $\Omega = 1.5$

Notes: (a) Time history; (b) spectrum plot; (c) phase portrait; (d) poincaré map

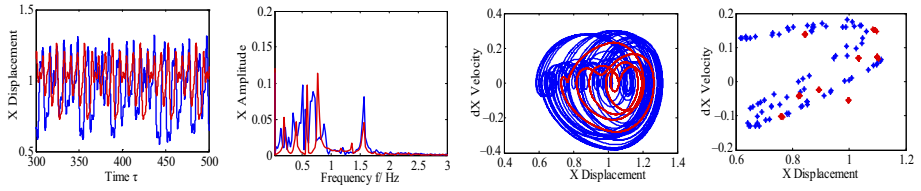

Figure 40. System response at $\Omega = 1.56$

Notes: (a) Time history; (b) spectrum plot; (c) phase portrait; (d) poincaré map

static transmission error, adhesion torque and tooth face friction and then carries out a numerical analysis of the system. Though adopting Ishikawa formula method, the comprehensive meshing stiffness is performed, where the results is compared by energy method. Based on the actual meshing contact location, tooth surface friction torque are both derived. Additionally, the adhesion-slip character of wheel/rail is analyzed to obtain the adhesion torque. Exciting frequency Ω, load torque T_2, gear backlash D, error fluctuation F_a and friction coefficient u_B are used as control parameters to investigate the influences on the dynamic behaviors of the traction system. The system responses are discussed and analyzed by time history, bifurcation diagram, spectrum plot, Poincaré map phase portrait and three-dimensional frequency spectrum.

The numerical results represent that the traction system goes through complex motion states including period-one, multi-period and chaos when exciting frequency changes. Furthermore, the bifurcation characteristics of system using exciting frequency as control parameter under Cases I and II are notably different. To ensure locomotive running steadily and reliably, the adhesion condition between wheel and rail should always lie in Case I. The varying gear backlash could switch the state responses of system, even causing the chaotic motion. Likewise, as error fluctuation increases, the motion forms of system starts with periodic motion, and then chaos, and finally, goes back to periodic motion. However, when error fluctuation is major, the system may be still under the unstable state because of severe vibration. As friction coefficients u_B increases, the window of chaotic motion becomes narrow and the vibration amplitude decreases. Thus, the proper value of system parameters should be specified so that the vibration amplitude can be reduced and the chaos even can be avoided.

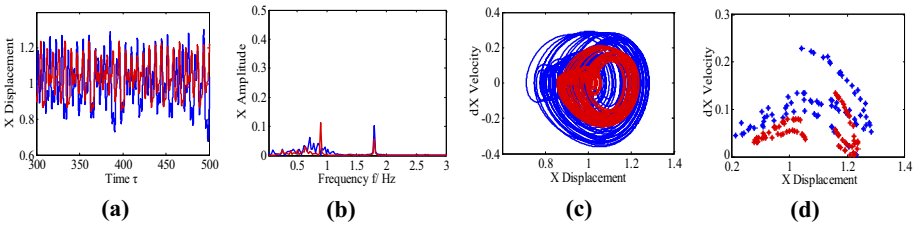

Figure 41.
System response at $\Omega = 1.8$

Notes: (a) Time history; (b) spectrum plot; (c) phase portrait; (d) poincaré map

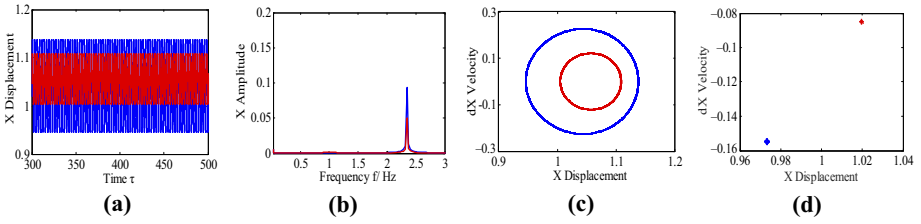

Figure 42.
System response at $\Omega = 2.4$

Notes: (a) Time history; (b) spectrum plot; (c) phase portrait; (d) poincaré map

References

Cao, J., Zhao, X.Y., Li, X.F., Lin, F. and Yang, Z.P. (2016), "Research on torsional vibration in traction drive system of high-speed train", *6th International Conference on Mechatronics, Materials, Biotechnology and Environment*, pp. 159-164.

Chang-Jian, C.W. (2013), "Micropolar fluid to improve dynamic response of gear pair system supported by journal bearings", *Engineering Computations*, Vol. 30 No. 5, pp. 628-647.

Chen, Z.G. and Shao, Y.M. (2011), "Dynamic simulation of spur gear with tooth root crack propagating along tooth width and crack depth", *Engineering Failure Analysis*, Vol. 18 No. 8, pp. 2149-2164.

Chen, Z.G., Zhai, W.M. and Wang, K.Y. (2017a), "A locomotive–track coupled vertical dynamics model with gear transmissions", *Vehicle System Dynamics*, Vol. 55 No. 2, pp. 244-267.

Chen, Z.G., Zhai, W.M. and Wang, K.Y. (2017b), "Dynamic investigation of a locomotive with effect of gear transmissions under tractive conditions", *Journal of Sound and Vibration*, Vol. 408, pp. 220-233.

Farshidianfar, A. and Saghafi, A. (2014a), "Global bifurcation and chaos analysis in nonlinear vibration of spur gear systems", *Nonlinear Dynamics*, Vol. 75 No. 4, pp. 783-806.

Farshidianfar, A. and Saghafi, A. (2014b), "Bifurcation and chaos prediction in nonlinear gear systems", *Shock and Vibration*, Vol. 2014, pp. 1-8.

Farshidianfar, A. and Saghafi, A. (2014c), "Identification and control of chaos in nonlinear gear dynamic systems using Melnikov analysis", *Physics Letters A*, Vol. 378 No. 46, pp. 3457-3463.

He, S., Cho, S. and Singh, R. (2008), "Prediction of dynamic friction forces in spur gears using alternate sliding friction formulations", *Journal of Sound and Vibration*, Vol. 309 No. 3/5, pp. 843-851.

He, S., Gunda, R. and Singh, R. (2007), "Effect of sliding friction on the dynamics of spur gear pair with realistic time-varying stiffness", *Journal of Sound and Vibration*, Vol. 301 No. 3/5, pp. 927-949.

Huang, G., Zhou, N. and Zhang, W. (2015), "Effect of internal dynamic excitation of the traction system on the dynamic behavior of a high-speed train", *Proceedings of the Institution of Mechanical Engineers, Part F: Journal of Rail and Rapid Transit*, Vol. 230 No. 8, pp. 1-9.

Kahraman, A. and Singh, R. (1990), "Non-linear dynamics of a spur gear pair", *Journal of Sound and Vibration*, Vol. 142 No. 1, pp. 49-75.

Kahraman, A. and Singh, R. (1991), "Interactions between time-varying mesh stiffness and clearance non-linearities in a geared system", *Journal of Sound and Vibration*, Vol. 146 No. 1, pp. 135-156.

Li, Y.G., Chen, T.N. and Wang, X.P. (2014), "Non-linear dynamics of gear pair with dynamic backlash subjected to combined internal and external periodic excitations", *Journal of Vibration and Control*, Vol. 22 No. 6, pp. 1693-1703.

Li, Y.P., Sun, W., Wei, J. and Chen, T. (2010), "Study on the improved algorithm of the time-varying meshing stiffness of gear", *Journal of Mechanical Transmission*, Vol. 34 No. 5, pp. 22-26.

Lu, F.X., Wang, H.F., Zhu, R.P., Bao, H.Y. and Jiang, H.H. (2015), "Dynamics characteristic analysis of spur gear pairs based on tooth surface friction", *Journal of Mechanical Transmission*, Vol. 39 No. 11, pp. 27-32.

Moradi, H. and Salarieh, H. (2012), "Analysis of nonlinear oscillations in spur gear pairs with approximated modelling of backlash nonlinearity", *Mechanism and Machine Theory*, Vol. 51, pp. 14-31.

Qin, D.T., Bai, W.Y. and Zhang, F.P. (2015), "Dynamic characteristic analysis of gear transmission system of wind turbine during braking process", *Acta Energiae Solaris Sinica*, Vol. 36 No. 2, pp. 305-312.

Shen, Y.J., Yang, S.P. and Liu, X.D. (2006), "Nonlinear dynamics of a spur gear pair with time-varying stiffness and backlash based on incremental harmonic balance method", *International Journal of Mechanical Sciences*, Vol. 48 No. 11, pp. 1256-1263.

Shi, J.L., Ma, X.G., Xu, C.L. and Zang, S.J. (2013), "Meshing stiffness analysis of gear using the Ishikawa method", *Applied Mechanics and Materials*, Vols 401/403, pp. 203-206.

Tamminana, V.K. and Kahraman, A. (2006), "A study of the relationship between the dynamic factors and the dynamic transmission error of spur gear pairs", *Journal of Mechanical Design*, Vol. 129 No. 1, pp. 75-84.

Tian, X. (2004), *Dynamics Simulation for System Response of Gearbox Including Localized Gear Faults*, University of Alberta, Edmonton.

Vaishya, M. and Singh, R. (2001a), "Analysis of periodically varying gear mesh systems with Coulomb friction using Floquet theory", *Journal of Sound and Vibration*, Vol. 243 No. 3, pp. 525-545.

Vaishya, M. and Singh, R. (2001b), "Sliding friction-induced non-linearity and parametric effects in gear dynamics", *Journal of Sound and Vibration*, Vol. 248 No. 4, pp. 671-694.

Walha, L., Fakhfakh, T. and Haddar, M. (2006), "Backlash effect on dynamic analysis of a two-stage spur gear system", *Journal of Failure Analysis and Prevention*, Vol. 6 No. 3, pp. 60-68.

Wan, Z.G., Cao, H.R., Zi, Y.Y., He, W.P. and He, Z.J. (2014), "An improved time-varying mesh stiffness algorithm and dynamic modeling of gear-rotor system with tooth root crack", *Engineering Failure Analysis*, Vol. 42, pp. 157-177.

Wang, J., Lim, T.C. and Li, M.F. (2007), "Dynamics of a hypoid gear pair considering the effects of time-varying mesh parameters and backlash nonlinearity", *Journal of Sound and Vibration*, Vol. 308 Nos 1/2, pp. 302-329.

Wang, K.Y., Zhai, W.M. and Chen, Z.G. (2016), "Numerical investigation on wheel-rail dynamic vibration excited by rail spalling in high-speed railway", *Shock and Vibration*, Vol. 2016, pp. 1-11.

Wang, J., Zhang, J.H. and Yang, A.B. (2012), "An analytical study of bifurcation and chaos in a spur gear pair with sliding friction", *Procedia Engineering*, Vol. 31, pp. 563-570.

Wang, J.G., He, G.Y., Zhang, J., Zhao, Y.X. and Yao, Y. (2017), "Nonlinear dynamics analysis of the spur gear system for railway locomotive", *Mechanical Systems and Signal Processing*, Vol. 85, pp. 41-55.

Wang, Y., Liu, J.X., Li, Y.F., Yu, D.L. and Xie, M. (2017), "Parametric vibration stability of locomotive gear transmission system with tooth surface friction", *Journal of Traffic and Transportation Engineering*, Vol. 17 No. 2, pp. 52-63.

Xu, S., Zeng, F.L. and Zhang, S.L. (2013), "Dynamic response analysis of transmission gear system with backlash", *Agricultural Equipment and Vehicle Engineering*, Vol. 51 No. 6, pp. 1-4.

Yao, Y., Zhang, H.J., Li, Y.M. and Luo, S.H. (2011), "The dynamic study of locomotives under saturated adhesion", *Vehicle System Dynamics*, Vol. 49, pp. 1321-1338.

Yao, Y., Zhao, S.Y., Xiao, F.X. and Liu, J.X. (2015), "The effects of wheel set driving system suspension parameters on the re-adhesion performance of locomotives", *Vehicle System Dynamics*, Vol. 53 No. 12, pp. 1935-1951.

Zhai, W.M., Cai, C.B., Zhang, N. and Wang, K.Y. (2013), "High-speed train–track–bridge dynamic interactions – part I: theoretical model and numerical simulation", *International Journal of Rail Transportation*, Vol. 1 Nos 1/2, pp. 3-24.

Zhang, T., Chen, Z.G., Zhai, W.M., Wang, K.Y. and Wang, H. (2019a), "Effect of the drive system on locomotive dynamic characteristics using different dynamics models", *Science China Technological Sciences*, Vol. 62 No. 2, pp. 308-320.

Zhang, T., Chen, Z.G., Zhai, W.M., Wang, K.Y. and Wang, H. (2019b), "Establishment and validation of a locomotive–track coupled spatial dynamics model considering dynamic effect of gear transmissions", *Mechanical Systems and Signal Processing*, Vol. 119, pp. 328-345.

Zhao, H.Y., Liu, J.X. and Zhai, W.M. (2009), "Simulation and analysis for self-excited torsional vibration of locomotive drive system", *Second International Conference on Transportation Engineering*, Vol. 345, pp. 1045-1050.

About the authors

Yan Xia is a PhD student at School of Mechanical Engineering, Shandong University, China. He received his master's degree from Northeastern University, China, in 2017. Now, his current research interests include the dynamics of structures and vibration control.

Yi Wan is currently a professor at the School of Mechanical Engineering, Shandong University, China. He received his PhD degree from Shandong University, China, in 2006. His main research interests include mechanical vibration, micro-milling and dynamics and control of the robot. Yi Wan is the corrosponding author and can be contacted at: wanyi@sdu.edu.cn

Hongwei Wang is a MD-PhD student at the School of Mechanical Engineering, Shandong University, China. His research interests include mechanical dynamics and topology optimization.

Zhanqiang Liu is currently a professor at the School of Mechanical Engineering, Shandong University, China. He received his PhD degree from the City University of Hong Kong in 1999. His main research interests include machine tool dynamics, high-speed machining, micro-manufacturing and process mechanics.